JOURNAL OF PROPULSION AND POWER
Vol. 36, No. 5, September–October 2020

Diode Laser Ignition of a Poly(Methyl Methacrylate) and Gaseous Oxygen Hybrid Motor

David M. Dyrda,* Flora S. Mechentel,* and Brian J. Cantwell†
Stanford University, Stanford, California 94305
and
Ashley C. Karp,‡ Jason Rabinovitch,§ and Elizabeth T. Jens‡
Jet Propulsion Laboratory, California Institute of Technology, Pasadena, California 91109

https://doi.org/10.2514/1.B37832

The performance of a diode laser igniter as a restart-capable device has been assessed for single-port, poly(methyl methacrylate) (PMMA)/gaseous oxygen (GOX) hybrid motors. For this testing a prototype version of the igniter has been designed and implemented as a substitute to a traditional methane/GOX torch ignition system. Ignition tests have been conducted at atmospheric ambient conditions using an experimental single-port motor setup. Using three PMMA fuel grains, a total of 46 successful motor ignitions and restarts were achieved. These tests were conducted using a single multimode diode laser with an output power of 10.84 W and a nominal pulse length of 1 s. In addition, a total of 24 successful ignitions and restarts were demonstrated in a vacuum chamber with the same prototype igniter on a flight-scale PMMA/GOX motor under development for smallsat applications. The ignition transient is compared against baseline results from a torch ignition system for atmospheric tests, and the ignition delay performance is considered across all tests.

I. Introduction

HYBRID motors use propellants stored separately and in different phases, producing a propulsion device that has a number of inherent advantages. By combining solid and liquid/gaseous propellants, there is a larger activation energy required for motor ignition, effectively eliminating the risk of a large chemical explosion. Furthermore, by placing a control valve between the two propellants the oxidizer flow can be stopped, thereby extinguishing combustion over the solid fuel grain. As a result, hybrid systems are frequently characterized as inherently restart-capable; however, motor reignition is accomplished only with a reusable igniter. In addition, the greater ignition energy requirements for mixed-phase propellants can lead to difficulties in igniting hybrid motors. To date, most hybrid motor development has occurred through research or sounding rockets where there is no need for reignition [1]. As a result, the task of developing and testing lightweight, reliable, restart-capable igniters has not been a priority.

In recent years, development of hybrid propulsion systems for in-space applications has confirmed the importance of restart-capable igniters. As a primary example, hybrid motor development being led by A. Karp and E. Jens for application to the CubeSat and broader microsatellite market has the potential to provide a wider range of impulsive maneuvering capabilities to a range of spacecraft in need of numerous trajectory changes [2]. Furthermore, the applicability of this type of propulsion device is only expected to grow. DelPozzo et al. project a rapid growth in the microsatellite industry (10–100 kg total mass), with an anticipated 2000–2800 microsatellite launches over the next 5 years [3]. A greater number of small, inexpensive satellites will in turn generate an increasing demand for smaller propulsion units capable of delivering impulsive maneuvers for a wide variety of applications. Perhaps the most notable emerging application is the concept of an interplanetary CubeSat. The small, standardized CubeSat configuration enables more affordable science, but a lack of existing small propulsion systems limits its mobility [2,4]. Combining the advantages of CubeSats with the large impulsive delta-V capabilities of a hybrid propulsion system could enable more affordable orbiting science in our solar system [5,6]. For example, an orbit insertion around Mars requires an approximate delta-V of 1 km/s when including subsequent trajectory cleanup maneuvers. Reference mission studies have demonstrated that hybrid propulsion systems using low-regression-rate thermoplastic fuels can outperform liquid monopropellant systems in terms of cost and payload mass delivered for these types of missions [2]. A major caveat is that, for this mission architecture, hybrid motors must be capable of performing up to approximately 10 motor restarts.

As a result, successful hybrid propulsion development for microsatellite applications hinges around the motor's ability to perform a number of relights without severely reducing its performance by adding too much mass to the system. A class of igniter that is widely used for this task on hybrid motors is referred to as a gas torch ignition system. This igniter uses gaseous fuel, gaseous oxidizer, and a spark plug to initiate a pilot flame that ignites the primary combustion chamber [7]. Torch igniters are commonly mounted on the front end of the combustion chamber, and the pilot flame enters the motor through a port. This type of igniter is effective and easily tailored to any propellant combination, but requires a secondary gaseous fuel to be carried onboard and adds extra tubing, hardware, and an additional control valve. Furthermore, this type of ignition system is the only well-tested option for restarting the propellant combination considered in this study (poly[methyl methacrylate]/gaseous oxygen, PMMA/GOX), demonstrating the gap in igniter technology that is present for hybrid motors. This has prompted a number of ignition studies in recent years that have aimed to develop novel technologies with low overall mass and complexity. One notable area of research has focused on the use of fuel additives to enable hypergolic ignition in hybrid motors. This work has largely been limited to wax-based fuels and other binders such as various epoxies and hydroxyl-terminated polybutadiene due to the ease of introducing fuel additives in the laboratory [8–12]. Another concept uses catalytic reactions of the oxidizer to produce oxygen and heat through an exothermic decomposition reaction. This, however, relies on a compatible oxidizer such

Presented as Paper 2019-4095 at the 2019 AIAA Propulsion and Energy Forum/EATS 2019, Indianapolis, IN, August 19–22, 2019; received 25 September 2019; revision received 27 March 2020; accepted for publication 23 April 2020; published online 27 May 2020.

*Ph.D. Candidate, Department of Aeronautics and Astronautics, 496 Lomita Mall. Member AIAA.
†Edward C. Wells Professor, Department of Aeronautics and Astronautics, 496 Lomita Mall. Fellow AIAA.
‡Propulsion Engineer, JPL Propulsion and Fluid Flight Systems, 4800 Oak Grove Drive, M/S 125-211. Senior Member AIAA.
§Mechanical Engineer, Entry, Descent & Landing and Formulation Group, 4800 Oak Grove Drive, M/S T1708-112. Senior Member AIAA.

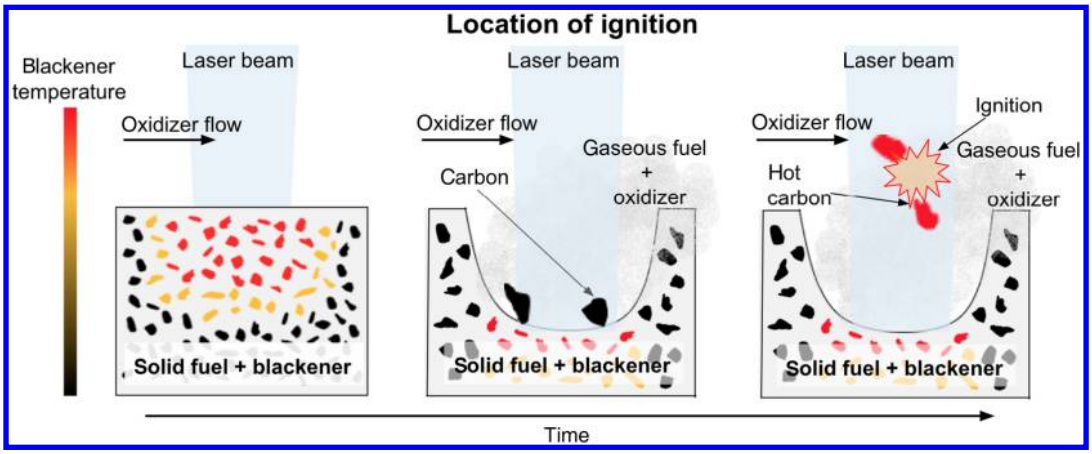

Fig. 1 The stages of diode laser ignition shown sequentially [16].

as hydrogen peroxide [13–15] or nitrous oxide [13]. Yet, for a wide range of possible hybrid motor propellant combinations (specifically classical thermoplastic fuels and GOX), there is no existing research into techniques that are more efficient than the torch igniter.

To address this issue, the current paper presents results from ignition tests conducted on two separate single-port, PMMA/GOX motors using a novel diode laser ignition system. The primary goal of these tests was to assess the reliability and restart capability of such a device. Ignition tests have been conducted at both atmospheric and vacuum exit conditions. As a means of assessing the ignition performance of the laser system, several tests have been compared against results from a torch ignition system equipped on the same motor. In total, this work comprises the demonstration of 70 successful laser ignitions (hot fires) over the course of 78 ignition tests.

Finally, the design for this igniter is based on previous results obtained from laser ignition tests conducted in a slab-burning combustion chamber that mimics hybrid motor combustion (consult Ref. [16]). These tests have demonstrated that a diode laser can be used to locally heat the surface of a blackened solid fuel, generating gaseous fuel through pyrolysis. This pyrolysis process leaves behind solid carbon content that is further heated by the laser while undergoing an oxidizer-driven entrainment process, physically moving these hot carbon particles to the location of a flammable propellant mixture for ignition. This process is depicted in Fig. 1. The solid carbon content can be char that is produced during pyrolysis, or it can be a carbon-based powder (carbon black, graphite, etc.) added during fuel grain casting. In terms of ignition performance, this mechanism produces shorter ignition delays in a faster oxidizer flow (due to faster particle movement), and when increasing the laser beam intensity (due to creating a greater number of hot carbon particles). Finally, this ignition process is effectively independent of wavelength due to the broadband absorbance of the blackener (carbon black) and the residual solid carbon across both the visual and near-infrared portions of the electromagnetic spectrum. The result of ignition through this mechanism is a localized flame kernel that is attached to the fuel grain surface at the location where the laser energy is absorbed.

II. Experimental Setup

A. Atmospheric Testing

1. *Integration of the Laser Igniter*

A cross-sectional view of the experimental motor used for atmospheric condition testing is presented in Fig. 2. It features an axial injector and a standard single-port geometry that includes small pre- and postcombustion chambers. The motor is composed of an optically transparent, square PMMA fuel grain that doubles as the combustion chamber and is sandwiched between two stainless steel end plates. This enables direct viewing of the full motor port throughout the entire duration of a test. In this setup the oxidizer flow rate is set to a constant value using a proportional-integral-derivative-controlled pressure feedback regulator system (Tescom ER5000/44-4000) along with a downstream choked orifice that can be swapped out. A Coriolis flow meter (Micro Motion CMFS025) provides real-time mass flow rates with an accuracy of 0.25% of the measurement. Chamber pressure data are acquired at the front and back end of the motor with four pressure measurements using Lord Sensing (Stellar Technology) GT1600-500A transducers (0.1% full-scale output accuracy = 3 kPa). As shown in Fig. 2 the topmost of the three fore-end ports is used as an entrance into the motor for the igniter. This motor was originally designed to be equipped with a torch igniter that produces a pilot flame that enters the combustion chamber through this port, impinging on the front face of the fuel grain at the location marked. For a more detailed description of this motor, consult Ref. [7].

For the purposes of running laser ignition tests, the torch igniter was removed and the same fore-end port was used as the entrance for the laser. The laser igniter consists of two main components: the laser system that gets attached to the motor, and a charring fuel with a trace

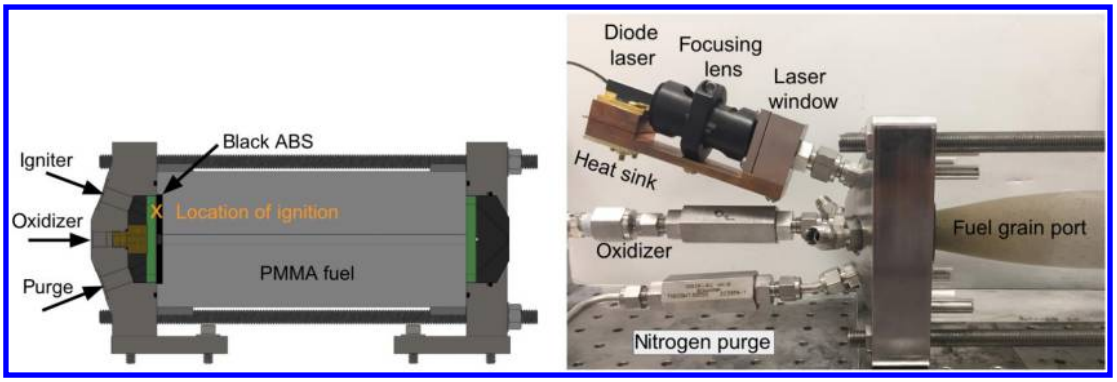

Fig. 2 Left: Experimental PMMA/GOX hybrid motor used to conduct laser ignition testing at atmospheric conditions. Right: The igniter mounting scheme is shown.

amount of a carbon black fuel additive for enhanced optical absorption. The igniter operates by sending a straight, focused beam of energy through the motor port such that it is absorbed at the surface of the blackened fuel. In addition, axial oxidizer injection in this motor will lead to recirculating or entrained oxidizer in the precombustion chamber that is needed to create the conditions for ignition as depicted in Fig. 1 [17].

For this set of experiments a small annular disk was cut out of the front face of the clear PMMA fuel grain and an annular disk of blackened acrylonitrile butadiene styrene plastic (ABS) of the same size (6.35 mm thick and 45 mm in diameter) was fit into this hole. The angle and path of the laser in this case is dictated by the existing igniter port, and so the diameter of this ABS disk was chosen to encompass the location of laser absorption, while its thickness was chosen so that a large number of motor restarts could be achieved before burning a hole through the ABS. The heating rate from the laser during these tests is the same order of magnitude as the rate of heat transfer during steady combustion of a thermoplastic fuel with GOX [18]. As a result, the rate of laser ablation is comparable to the regression rate of the fuel (typically a fraction of a millimeter/second), allowing for at least 10 restarts. In a general hybrid motor setup it may be possible to substitute far less of the fuel grain, as dictated by the laser beam size during absorption.

The laser and optical system component of the igniter is shown mounted on the motor in Fig. 2. The laser is a 16 W, continuous-wave diode laser, emitting at a center wavelength of 1064 nm, from Eagleyard Photonics (part number EYP-BAL-1064-16000-4020-CDL02-000). A laser capable of emitting several watts is essential to heating and vaporizing a solid thermoplastic fuel grain. This package includes a set of integrated microcollimating lenses that reduce the beam's half-angle divergence to 1.5 deg. The beam's size is further controlled using a single focusing lens, chosen according to the distance between the laser and the fuel grain surface; in this case a focal length of 200 mm was used. The main laser beam parameter of interest in this application is the beam intensity, which can be controlled by adjusting either the output power or beam area. The laser beam passes through a hermetically sealed window assembly that contains a 25-mm-diam, near-infrared, antireflective-coated fused silica window, 5 mm in thickness. The mounting of the laser window resulted in an optical path that was approximately 70 mm from the window interior to the entrance of the combustion chamber and cylindrical in shape with a minimum diameter of 7.5 mm. In this configuration, the laser beam crosses the blackened ABS fuel disk at a 15 deg angle. All of these components are mounted together on a copper platform that doubles as a passive heat sink for the laser. A mass and volume breakdown for the igniter is provided in Table A1 in the Appendix. The goal of this laser system was to establish a baseline design that exhibits the lightweight and compact qualities of this class of igniter. For these tests, power is supplied to the laser using a regulated power supply. In application, a high current can be supplied by a capacitor discharge device for each laser pulse.

2. *Test Conditions*

A total of 49 short ignition tests were conducted on this motor. These tests were performed on three fuel grains, with 24 tests conducted on the first fuel grain, 14 on the second fuel grain, and 11 on the third fuel grain. Three separate restart capability tests were conducted: hot fires 1–17 on fuel grain 1, 1–10 on fuel grain 2, and 1–9 on fuel grain 3. During each of these restart test series the motor and igniter were not altered between tests in an effort to mimic conditions for a CubeSat application.

Throughout these tests the two main laser parameters (output power and beam size during absorption) were held constant to assess igniter reliability at a single beam intensity. The beam area used for all tests on fuel grains 1 and 2 was 3.93 ± 0.05 mm^2 and for fuel grain 3 was 4.30 ± 0.05 mm^2 (the focusing lens was removed, because it was not playing a critical role in this particular setup). An initial test was conducted at a laser output power of 7.00 ± 0.21 W (beam intensity: 1.8 ± 0.1 W/mm^2). This test did not result in ignition, so the power was increased to 10.84 ± 0.33 W (beam intensity: 2.8 ± 0.1 W/mm^2) and remained at this setting for the remainder of the tests.

The oxidizer flow rate and steady-state combustion chamber pressure were the two motor parameters that were varied across each fuel grain. Restarts of the same fuel grain occurred at the same oxidizer mass flow rate, but at decreasing oxidizer mass fluxes and varying flow geometries as the port widened. Table A2 in the Appendix lists the initial port diameter for each fuel grain and average final port diameter computed from mass measurements. The ignition sequence was chosen such that the laser was always turned on either with or after the oxidizer. The motor operating conditions and ignition sequence for each test are provided in Table A3 in the Appendix.

During tests, high-speed video of combustion along the port was recorded at 5000 frames per second using a Photron Fastcam Mini AX100. The timing for the test sequence was handled through an Arduino Mega, and the camera was triggered with the laser enabling this footage to be synchronized against the chamber pressure data. In addition, the temperature of the diode laser element was monitored throughout testing using a surface-mounted thermistor.

Between tests, the laser igniter was removed from the motor to document the accumulation of soot on the interior side of the laser window. This window was not cleaned or altered in any way between tests so as to replicate the conditions for a continuous string of motor restarts. To ensure consistent conditions for ignition, a minimum spacing of 30 min between tests was maintained to allow the fuel grain to return to ambient conditions before the next test. This is also done to mimic the ignition conditions anticipated for CubeSat applications. As a result, these tests do not assess the thermal loading of the laser during a continuous run of closely spaced ignitions.

B. Vacuum Testing

1. *Integration of the Laser Igniter*

A cross-sectional view of the flight-scale motor used for ignition testing in vacuum is presented in Fig. 3. Although it features a similar overall geometry to the experimental motor, the fuel grain dimensions are marginally larger, and the pre- and postcombustion chambers are more prominent. The same laser igniter device was installed for these vacuum chamber tests and was mounted in an identical fashion, but at a steeper angle (again, as dictated by the existing igniter port). Similarly, the front of the clear PMMA fuel grain was replaced with blackened ABS fuel to facilitate ignition. Overall, these differences in the motor design will impact the internal flow dynamics. Ultimately, it is the local flow velocity near the location of ignition that influences the resulting ignition delay. In addition, a steeper laser angle will impact ignition as well, although the form and extent of this effect is currently unknown. Because of the inability to make visual observations within this motor, it was not possible to conclusively determine the impact of each of these factors. Rather, the primary goal of these tests was to make a first demonstration of laser ignition in vacuum. Additional details regarding this motor can be found in Ref. [19].

2. *Test Conditions*

A total of 29 short ignition tests were conducted in a vacuum chamber. These tests were performed on a single fuel grain and were aimed at demonstrating a large number of motor restarts in vacuum. The laser operating conditions were constant for all of these tests with the laser power set at 12.00 ± 0.36 W and a measured beam area at impact of 5.1 ± 0.5 mm^2 (beam intensity: 2.4 ± 0.3 W/mm^2).

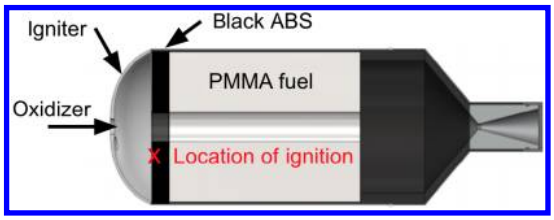

Fig. 3 PMMA/GOX hybrid motor used to conduct laser ignition testing in vacuum. The igniter mounting scheme is shown.

Compared with the atmospheric tests, the larger beam area used in this case was due to the difficulty of having to align the laser optics within the confined vacuum chamber. To account for this, the laser power was increased, resulting in a similar beam intensity. As presented in Table A4 in the Appendix, the ignition sequences in this case represent flight-like timing, with the laser turned on either with or before the oxidizer flow. The laser duration was tested at a maximum of 1 s and the hot fires each ran for between 1 and 5 s following ignition. The oxidizer flow rate for all tests was 6.7 g/s corresponding to a starting oxidizer mass flux of 15 $kg/(m^2 \cdot s)$. The time between tests was approximately 5 min, which was the minimum time requirement for the vacuum pump to bring the chamber to under 4 Pa. A longer spacing between tests to allow the motor to cool was not feasible given the expense of operating the vacuum chamber. For additional information on these tests, consult companion paper Ref. [19].

III. Discussion of Test Results

A. Reliability

1. Atmospheric Tests

The primary goal of these tests was to establish the operational capabilities of a diode laser igniter for a standard hybrid motor geometry. Of the 49 atmospheric tests, 46 of them resulted in successful ignition. Across all of these tests the igniter never failed when operating at a previously verified condition. An initial test conducted at an average beam intensity of 1.8 W/mm^2 did not produce ignition (unsuccessful test on fuel grain 1), whereas later tests demonstrated highly reliable performance using 2.8 W/mm^2. Furthermore, reliable ignition was observed down to a 200 ms pulse from the laser, corresponding to ~2.2 J of ignition energy. This value is comparable to minimum ignition energies reported for other hybrid motor ignition techniques under development [20]. The two unsuccessful tests on fuel grain 3 were the result of reducing the laser pulse below 200 ms. Successful tests were conducted for averaged oxidizer mass fluxes ranging from approximately 4 to 110 $kg/(m^2 \cdot s)$. Across these tests the average chamber pressure following ignition and during quasi-steady operation ranged from 441 to 752 kPa. Furthermore, this testing demonstrated that the laser ignition scheme is reliable across a range of ignition sequences. Initially, the laser was turned on once the flow in the motor reached a steady state, whereas later tests demonstrated that the igniter can also operate during the initial transient oxidizer fill period.

2. Vacuum Tests

Of the 29 vacuum tests, 24 resulted in successful ignition. During test 1 the oxidizer valve did not open. No ignition during test 2 was the result of not leaving the laser on for long enough, which was corrected in test 3. During test 13 the laser was purposefully not turned on, leading to no ignition, whereas in test 14 there was purposefully no overlap between laser and oxidizer, again preventing ignition. These two tests ruled out the possibility of an elevated fuel grain temperature producing ignition on its own (autoignition). Only one of the failed tests (test 18) was due to the laser system not producing ignition at a previously tested operating condition. During vacuum testing, ignition was demonstrated for laser pulses as short as 50 ms, corresponding to ~0.6 J of ignition energy. However, this condition was less reliable (as demonstrated by test 18), prompting the final string of ignitions with a beam pulse of 200 ms (2.4 J). Tests were carried out at oxidizer mass fluxes ranging from about 4 to 15 $kg/(m^2 \cdot s)$, and the average chamber pressure following ignition and during quasi-steady operation fell between 848 and 1179 kPa. By running experiments in two motors this ignition scheme has been shown to be reliable with both a small (atmospheric tests) and more traditionally sized (vacuum tests) precombustion chamber. Tests in vacuum demonstrate that the igniter can be turned on either before or simultaneously with the oxidizer. This result is of key practical importance to the implementation of this igniter for space applications where it is advantageous to avoid an unnecessary waste of oxidizer.

B. Restart Capability

1. Atmospheric Tests

The ability to burn a hybrid motor numerous times is a core aspect of its usefulness as a propulsion device in space. Therefore, demonstrating a large number of restarts with this igniter was a second important goal of these tests. Figure 4 presents a series of artificially combined combustion chamber pressures from the restart tests conducted on fuel grain 1 (hot fires 1–17). This result is representative of all three restart test series. In each case, the motor was fully ignited and reached the expected chamber pressure, even demonstrating the same trend of increasing chamber pressure observed during long-duration burns of this motor.

The laser igniter excelled at performing motor restarts despite a concern regarding soot accumulation on the laser window. Pictures of the laser window taken between each test revealed that soot was indeed reaching this window. The quantity of soot on the window did not steadily become greater, but instead fluctuated from test to test, suggesting that the flow structure near the window was both depositing and clearing soot from the window. The left-side image in Fig. 5 shows the heaviest soot coverage observed across all tests in this motor. The red circle in this image roughly indicates the size and location of the laser beam, an approximation that was possible to make given that the beam converges slowly in this application. Because the window was not cleaned between ignitions, reliable operation of the laser system has been demonstrated over a cumulative 163 s exposure to motor operation. Although some of the laser power would have been absorbed by this soot (not measured during these tests), the output power of the laser never had to be adjusted to account for this.

An additional concern was thermal management of the laser, which produces a large amount of heat during operation. The copper heat sink mount on the igniter was able to effectively hold the laser temperature within 1°C when operating the laser at a 1 s pulse. The temperature of the laser returned to the ambient temperature within approximately 30 s following shut off. This result is promising and suggests that the size of the heat sink could be drastically reduced, particularly if using a finned design.

2. Vacuum Tests

The series of ignition tests conducted in vacuum demonstrated that motor restart with this ignition scheme is feasible in a more representative operating environment for space missions. As a point of reference, these 24 motor restarts in vacuum represent two times the anticipated amount needed to implement a CubeSat mission architecture for Mars orbit insertion [2]. Based upon an observation of the laser window following the entire set of tests (right image in Fig. 5),

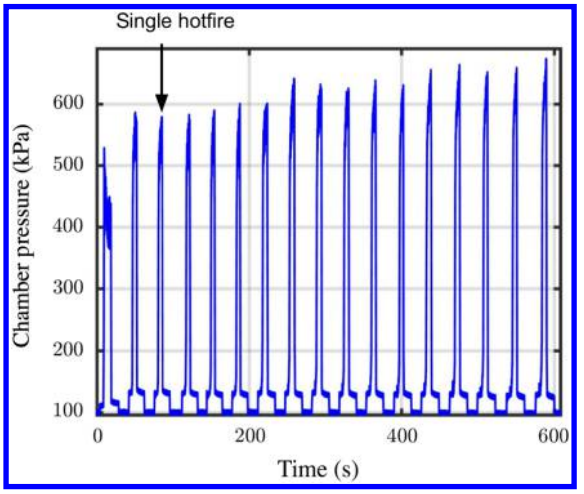

Fig. 4 Hot fires 1–17 on fuel grain 1, intended to mimic a series of restarts without motor adjustment. Chamber pressure data from individual tests have been stitched together.

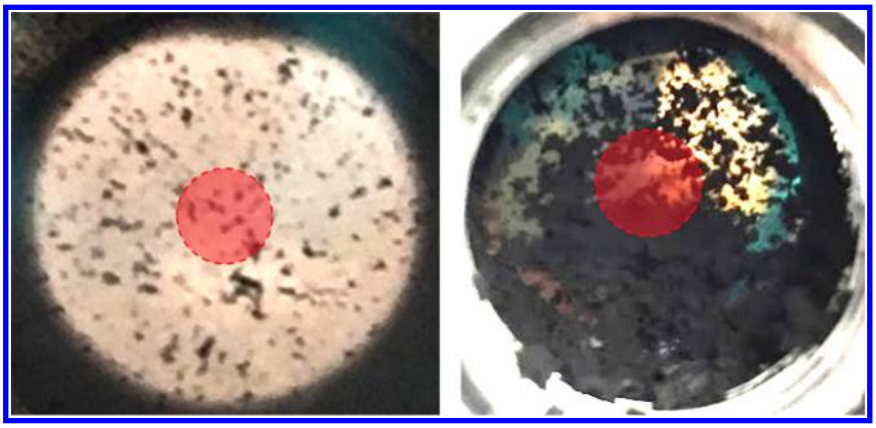

Fig. 5 Soot on the laser window following restart tests at atmospheric conditions (left) and vacuum conditions (right). Approximate laser position and size indicated (red).

it was found that far more soot was present during the vacuum ignitions. This is because a larger section of ABS (a char-producing material) was used in this motor for ignition. From the level of soot found on this window, it is suspected that the use of a relatively large beam area during these tests helped contribute to a high level of ignition reliability by spreading out the delivered energy, thereby mitigating the risk of a single point of failure caused by soot coverage. Again, the output power of the laser never had to be adjusted to compensate for this soot coverage.

C. Ignition Transient

1. *Atmospheric Tests*

The chamber pressure ignition transient generated by the laser igniter during atmospheric condition tests is compared in Fig. 6 against results from a torch igniter on the same motor at comparable times into the operation of the motor. The oxidizer flow rate is identical for all tests shown, and a slightly different nozzle throat area leads to a different steady-state chamber pressure in each comparison, but does not have a large impact on chamber pressure at the time of ignition. Finally, the data for each test comparison are reported such that the steep chamber pressure increases are aligned, emphasizing the similarity in pressure rise before this time.

The results from both igniters share a number of similarities. First, the overall shape of the transients in each instance is similar. Furthermore, results from both igniters produce broader ignition events as the port widens during motor operation. Comparing these chamber pressure traces against the synchronized high-speed camera footage, the broadening of the ignition transient results from an evolving flow geometry affecting the process of flame propagation along the port. In particular, the motor used during testing forms a bulge near the center of the port as a result of uneven fuel regression. The series of images in Fig. 7 provide a visual of the flame as it spreads through this bulge, which accounts for a sizable portion of the ignition delay on this motor. The similarity in shape of the ignition transients suggests that both devices are locally igniting the fuel grain on or near its front face, after which full motor ignition occurs through a process of flame propagation driven by the flow in the motor.

These results also suggest a number of differences between the two igniters. In particular, for these three tests the ignition delay from the laser igniter appears to vary by several seconds. A portion of this variation is due to the increase in time needed to ignite the port as the fuel grain regresses, whereas the remainder is due to an additional effect that can be traced back to the laser ignition mechanism. Looking at the laser ignition transient from fuel grain 1, hot fire 15 (Fig. 7), it is clear that this curve is initially flat before gradually increasing as the port ignites. Comparing against the high-speed camera data, no flame is observed in the port throughout this entire period, suggesting that this feature corresponds to the laser ignition event in the precombustion chamber. As will be discussed in more detail in the next section, tests indicate that the variation in laser ignition delay is due to both of these features of the ignition transient. As a final note, it was observed that the laser igniter produced less chamber pressure fluctuation during the ignition process as compared with the torch igniter. This difference is presumably attributed to the fact that during laser ignition there is no additional mass being injected into the motor.

2. *Vacuum Tests*

Results obtained from vacuum ignition tests also support the conclusions discussed in the previous section. Figure 8 presents results from two tests that show similar chamber pressure traces following widely different laser sequences. This suggests that the laser is responsible only for generating an initial flame kernel, after which point in time the ignition process is driven by the flow. Furthermore, it is notable that for many of the tests the igniter is active only while the motor is initially being filled with oxidizer (opening of the GOX valve corresponds to the start of the chamber pressure rise from 0 kPa for these tests). This means that the initial ignition event has already occurred well before the entire motor is

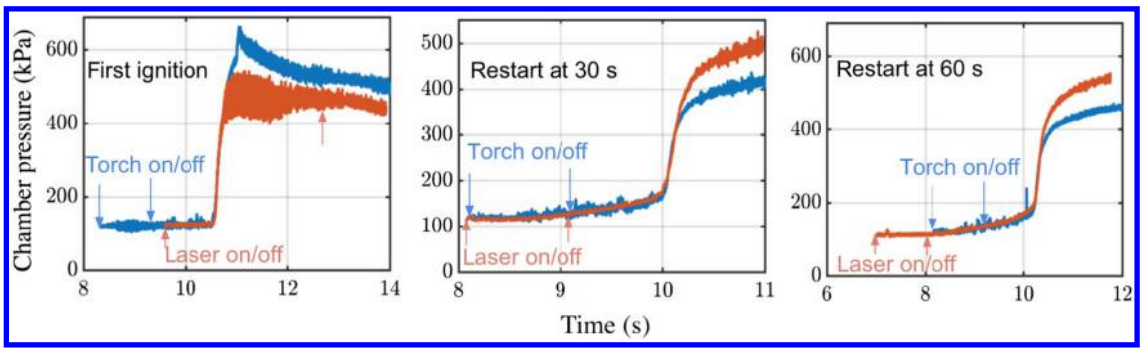

Fig. 6 Comparison of laser igniter (fuel grain 1 hot fires 1, 7, and 15) and torch igniter transients. Oxidizer flow is stabilized before ignition in all cases.

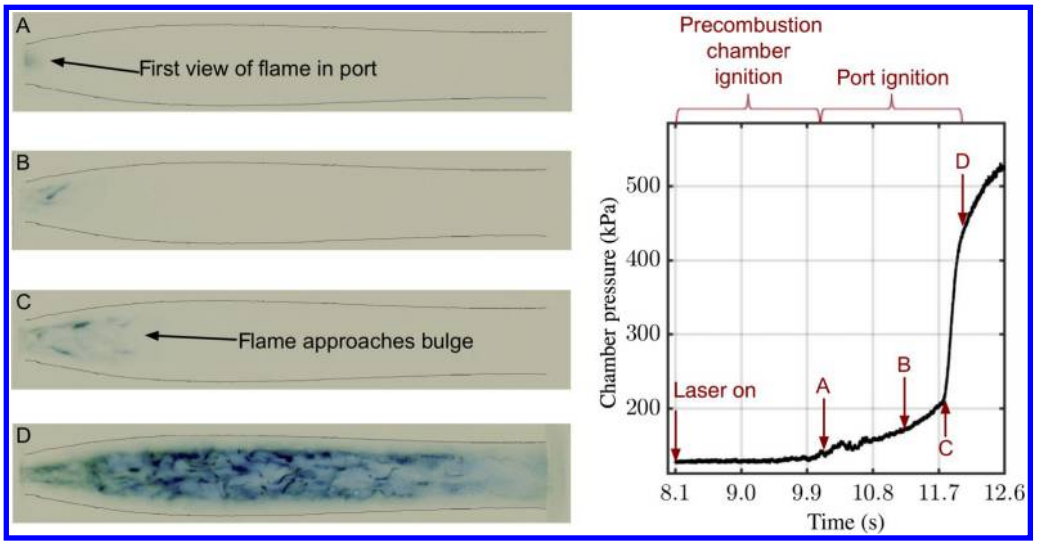

Fig. 7 Chamber pressure data from fuel grain 1 hot fire 15 presented alongside synchronized high-speed camera data (negative image) showing the ignition transient.

burning, a result that is consistent with the fact that the laser is producing ignition at a single point in the motor.

D. Ignition Delay

1. Atmospheric Tests

Ignition delay data have been compiled for each of the tests conducted during this study and are defined as the time between the laser turning on and the chamber pressure reaching 50% of its average quasi-steady value following ignition. Error bars are included with these values and indicate the duration of the primary chamber pressure rise. Figure 9 presents the ignition delays for the series of motor restart tests conducted on each fuel grain. The trend of increasing ignition delay observed in the previous section becomes even more apparent with these results. However, there is fluctuation in this trend and the additional observation that the ignition delay consistently drops immediately following the first ignition.

As previously discussed, the ignition transient is composed of an initial period during which the flame is initiated in the precombustion chamber, followed by the time required for the flame to catch throughout the entire port (see Fig. 7). From high-speed video data the duration of these two events has been determined for the restart tests on fuel grain 1 and is shown in Fig. 10. Both of these events demonstrate a tendency to increase as the port widens. However, the precombustion chamber portion appears to depart from a clean trend line quite drastically. Although ignition repeatability was not addressed in this study, these results suggest that the spread in ignition delay repeatability for this igniter would primarily be attributed to the initial laser ignition event. These results are consistent with a slab burner study aimed at assessing the influence of flow velocity on ignition delay for this laser ignition scheme, which found

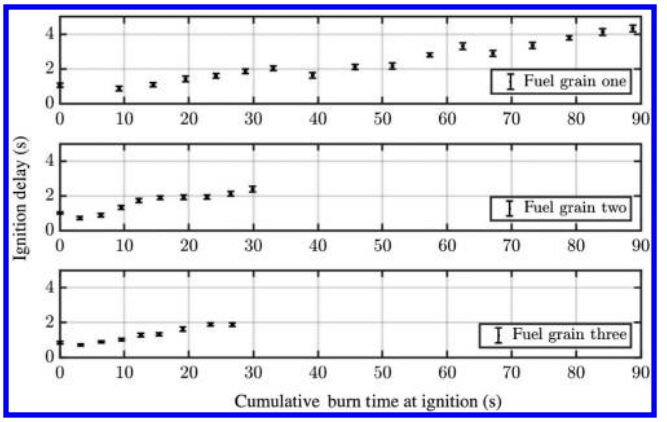

Fig. 9 Ignition delays compiled for restart ignition tests in atmospheric conditions. All three tests exhibited a trend of increasing ignition delay as the port widened.

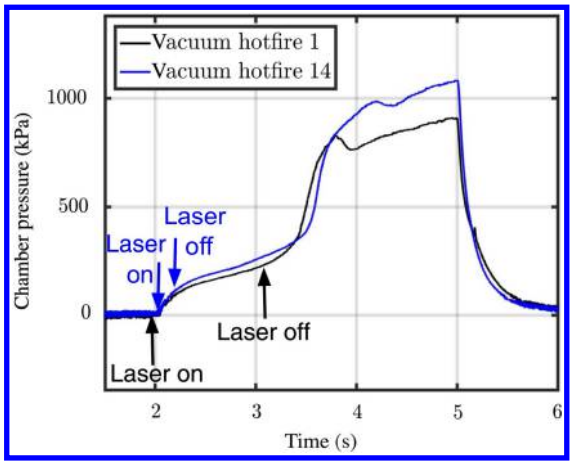

Fig. 8 Chamber pressure data from vacuum hot fires 1 and 14. Differing laser sequences have little effect on overall ignition transient.

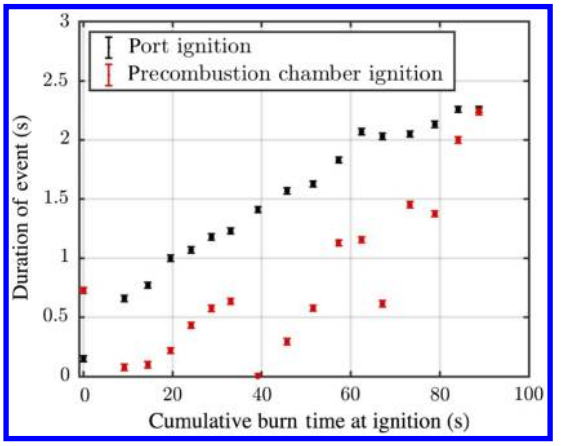

Fig. 10 Duration of the two ignition transient events for a laser ignition system (fuel grain 1).

that the time required to initiate combustion becomes larger and exhibits more variance as the local flow velocity decreases [16]. The variance in this process stems from the stochastic nature of the heated soot particle entrainment process that drives ignition. As the motor port opens throughout operation, the oxidizer velocity drops, leading to these issues.

From Fig. 10 it is also clear that the longer delay for the first motor ignition is due to the process of flame initiation in the precombustion chamber, a result that is suspected to be caused by an initially smooth fuel grain surface that results in a slower-traveling flame front. During subsequent tests the fuel grain has larger surface features that are thought to increase the rate at which the flame spreads by promoting surface flame holding. The observation of a longer first ignition delay has been consistent throughout this study, but unfortunately there was no visual access to the precombustion chamber to directly verify this claim.

To assess the extent to which the laser ignition delay is flow velocity driven, a series of five consecutive tests were performed at varying oxidizer flow rates. The ignition delays from these tests are presented in Fig. 11. To account for the effects of an increasing port diameter on consecutive tests, the higher flow rate tests should be compared with the constant flow rate trend line, which here is approximated as a linear trend for short burn times. The ignition delay was more than cut in half as a result of a 50% increase in oxidizer flow rate. Although this trend cannot continue indefinitely, these initial results indicate that this type of igniter would provide faster ignition in motors operating at higher flow rate conditions.

Finally, it is noted that ignitions have been demonstrated up to a cumulative burn time of about 110 s. For intended CubeSat applications the expectation is that a hybrid motor would be capable of producing thrust for 200 s or more, which means that laser ignition performance would still need to be assessed for the second half of the motor's lifetime. In addition, the duration of the hot fires following each ignition has been on the short end, perhaps corresponding to orbital adjustment maneuvers. Ignition following a much longer orbit insertion maneuver, for example, would require testing ignition following a longer burn duration. Fuel regression during a longer burn would have the tendency to produce a level surface for ignition, and so the expectation is that ignition should not be adversely affected.

2. *Vacuum Tests*

Ignition delay data from the vacuum ignition tests are presented in Fig. 12. These results serve to demonstrate that both the timescale of the ignition event and the general trends in delay remain unchanged in a vacuum environment. In particular, the longer ignition transient for the first motor test was clearly observed. However, these results show less variation in ignition delay as compared with the atmospheric tests, a result that likely stems from one or more of the differences between these two test setups as described in Sec. II.B.1. Unfortunately, without visual access to the motor, it has not been possible to conclusively determine the underlying cause of this variation.

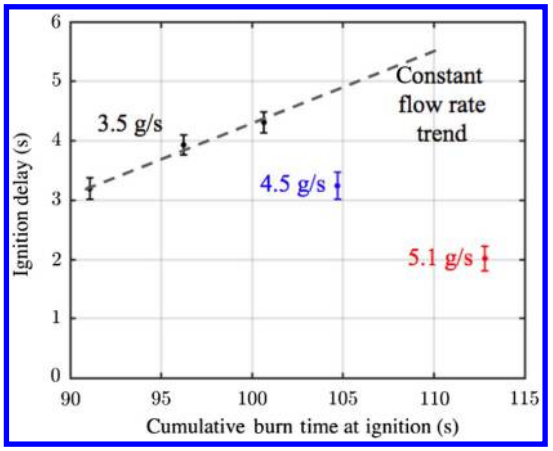

Fig. 11 Test results for hot fires 18–22 on fuel grain 1. Ignition delay exhibited a strong dependence on flow velocity.

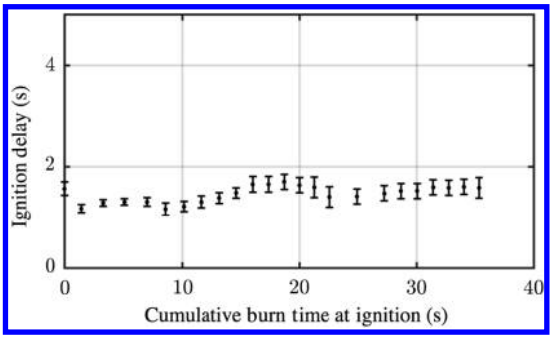

Fig. 12 Ignition delays compiled for restart tests in vacuum. Results are comparable to similar tests at atmospheric conditions.

IV. Conclusions

This work has established preliminary test results regarding the performance of a novel diode laser ignition system for hybrid motors. This ignition scheme uses a single-diode laser to heat a small area on the surface of the fuel grain. A prototype version of the igniter has reliably provided ignition on two separate motors over the course of 78 tests that have spanned a wide range of ignition sequences and motor conditions in both atmospheric and vacuum environments.

The ignition transient produced by this type of device occurs in two phases. Initially, the laser generates a small flame kernel in the precombustion chamber. As this flame spreads it is entrained into the port, causing ignition of the full motor. These tests have demonstrated that this entire ignition process is heavily dependent on the oxidizer flow within the motor, with higher flow rates producing faster ignition. As a result, the performance of this type of igniter must be characterized for its particular application.

In terms of device performance, laser ignition has been demonstrated when turning the laser system on before, with, or after the GOX valve. The ignition delay produced by this type of device has been shown to vary, although trends in the evolution of the ignition delay throughout the lifetime of a motor have been consistent across multiple test series aimed at assessing the restart capability of this device. As the port opens, the ignition delay has a tendency to increase, a result that is likely connected to a decreasing oxidizer velocity in the motor.

Given the variation observed in the ignition delay results, the authors believe that future work should focus on characterizing the repeatability of this device. Additionally, based on the heavy flow dependence of the ignition transient, it is expected that the oxidizer injection scheme will play a significant role in ignition performance; however, this is currently unconfirmed. Finally, current results suggest that attempting ignition directly in the port where a higher flow velocity is present may be a promising next step for reducing ignition delay with this device.

Acknowledgments

This work has been funded through the Center of Excellence for Aeronautics and Astronautics. This research has also been made possible with support from the NASA Jet Propulsion Laboratory through a Strategic University Research Partnership and from Stanford's School of Engineering. The authors would like to thank Godwin Zhang for supporting the experimental aspects of this project. Vacuum testing was performed at the Jet Propulsion Laboratory, California Institute of Technology, under a contract with NASA. Reference herein to any specific commercial product, process, or service by trade name, trademark, manufacturer, or otherwise does not constitute or imply its endorsement by the U.S. Government or the Jet Propulsion Laboratory, California Institute of Technology.

Appendix: Test Data

Table A1 Mass and volume breakdown of each of the components on the prototype laser system

Component name	Primary material	Mass, g	Volume, cm^3
Diode laser	Copper	26.1	2.9
Heat sink platform	Copper	258.5	29.3
Focusing lens assembly	Aluminum	52.2	19.3
Laser window assembly	Stainless steel	154.2	19.7

Table A2 Key dimensions for each of the fuel grains tested at atmospheric conditions

Fuel grain	Initial port diameter, mm	Average final port diameter, mm	Initial nozzle throat area, mm^2
1	6.35	32.6	13.0
2	6.35	21.7	14.1
3	12.7	22.5	22.4

Table A3 Laser ignition atmospheric test parameters

Fuel grain	Hot fire	Oxidizer flow rate, g/s	Chamber pressure, kPa	Laser start, s	Laser duration, s	Test duration, s	Ignition delay, s
1	Unsuccessful	3.49	N/A	4	3	0	N/A
1	1	3.49	441	4	3	9.2	1.05
1	2	3.50	531	4	1.5	5.3	0.88
1	3	3.51	524	4	1	5.0	1.09
1	4	3.51	524	4	1	4.7	1.42
1	5	3.50	538	4	1	4.6	1.60
1	6	3.50	538	4	1	4.3	1.85
1	7	3.51	552	4	1	6.1	2.04
1	8	3.51	586	4	1	6.5	1.64
1	9	3.52	579	4	1	5.8	2.11
1	10	3.52	579	4	1	5.8	2.16
1	11	3.58	586	4	1	5.1	2.80
1	12	3.53	586	4	1	4.7	3.31
1	13	3.52	607	4	1	6.1	2.90
1	14	3.54	614	4	1	5.7	3.35
1	15	3.48	614	4	1	5.2	3.78
1	16	3.49	614	4	1	4.6	4.13
1	17	3.53	627	4	1	5.6	4.33
1	18	3.47	386	4	1	5.2	3.20
1	19	3.49	393	4	1	4.4	3.93
1	20	3.48	386	4	1	4.0	4.31
1	21	4.48	524	4	1	8.1	3.24
1	22	5.11	607	4	1	9.3	2.03
1	23	5.12	614	4	1	8.5	2.87
2	1	4.47	752	4	1	3.1	1.00
2	2	4.51	662	4	1	3.3	0.71
2	3	4.54	614	4	1	3.2	0.87
2	4	4.50	586	4	1	2.7	1.32
2	5	4.49	586	4	1	3.3	1.73
2	6	4.51	586	4	1	3.7	1.88
2	7	4.52	593	4	1	3.6	1.92
2	8	4.54	607	4	1	3.6	1.93
2	9	4.52	614	4	1	3.4	2.12
2	10	4.50	655	4	1	8.6	2.38
2	11	4.49	490	4	1	21.0	2.31
2	12	4.50	524	4	1	21.5	1.79
2	13	4.49	545	4	1	21.6	1.66
2	14	4.49	531	4	1	6.5	1.71
3	1	9.22	731	4	1	3.2	0.84
3	2	9.36	752	4	1	3.3	0.71
3	3	9.25	745	4	1	3.1	0.88
3	4	9.31	731	4	1	3.0	1.01
3	5	9.27	710	4	0.5	2.8	1.26
3	6	9.35	717	4	0.4	3.7	1.32
3	7	9.35	696	0	0.3	4.3	1.623
3	8	9.30	669	0	0.2	3.1	1.90
3	Unsuccessful	9.233	N/A	0	0.1	0	N/A
3	Unsuccessful	9.26	N/A	0	0.15	0	N/A
3	9	9.22	634	0	0.2	3.4	1.88

Laser start is relative to oxidizer start.
N/A = not available.

Table A4 Laser ignition vacuum test parameters

Test number	Hot fire number	Chamber pressure, kPa	Laser start, ms	Laser duration, ms	Test duration, s	Ignition delay, s
1	Unsuccessful	N/A	−50	500	0	N/A
2	Unsuccessful	N/A	−50	500	0	N/A
3	1	848	−50	1000	1.4	1.56
4	2	862	−50	1000	1.9	1.17
5	3	889	−50	1000	1.8	1.28
6	4	910	−50	1000	1.9	1.30
7	5	972	−50	1000	1.6	1.30
8	6	1000	−50	800	1.6	1.16
9	7	1014	−50	600	1.5	1.21
10	8	1014	−50	400	1.5	1.30
11	9	1014	−50	200	1.4	1.38
12	10	1014	−50	100	1.4	1.48
13	Unsuccessful	N/A	−50	0	0	N/A
14	Unsuccessful	N/A	−50	50	0	N/A
15	11	1007	0	50	1.3	1.65
16	12	1007	−50	1000	1.65	3.78
17	13	1020	0	50	1.3	1.70
18	Unsuccessful	N/A	0	50	0	N/A
19	14	1034	0	200	1.3	1.63
20	15	1034	0	200	1.3	1.59
21	16	1110	0	200	2.4	1.40
22	17	1124	0	200	2.3	1.41
23	18	1062	0	200	1.4	1.47
24	19	1055	0	200	1.4	1.52
25	20	1041	0	200	1.4	1.52
26	21	1055	0	200	1.3	1.59
27	22	1055	0	200	1.3	1.58
28	23	1055	0	200	1.3	1.60
29	24	1179	0	200	4.4	1.58

Laser start is relative to oxidizer start.
N/A = not available.

References

[1] Alkuam, E., and Alobaidi, W., "Experimental and Theoretical Research Review of Hybrid Rocket Motor Techniques and Applications," *Advances in Aerospace Science and Technology*, Vol. 1, No. 3, 2016, pp. 71–82. https://doi.org/10.4236/aast.2016.13007

[2] Jens, E., Cantwell, B., and Hubbard, G., "Hybrid Rocket Propulsion Systems for Outer Planet Exploration Missions," *Acta Astronautica*, Vol. 128, Nov.–Dec. 2016, pp. 119–130. https://doi.org/10.1016/j.actaastro.2016.06.036

[3] DelPozzo, S., Williams, C., Doncaster, B., Carapaica, L., and Gerber, D., *2019 Nano/Microsatellite Market Forecast*, 9th ed., Space Works Enterprises, Atlanta, GA, 2019, pp. 3–8.

[4] Tummala, A., and Dutta, A., "An Overview of Cube-Satellite Propulsion Technologies and Trends," *Aerospace*, Vol. 4, No. 4, 2017, p. 58, Dec. 2017. https://doi.org/10.3390/aerospace4040058

[5] Maisonneuve, Y., Godon, J. C., Lecourt, R., Lengelle, G., and Pillet, N., "Hybrid Propulsion for Small Satellites: Design Logic and Test," *International Journal of Energetic Materials and Chemical Propulsion*, Vol. 5, Nos. 1–6, Jan. 2002, pp. 90–100. https://doi.org/10.1615/IntJEnergeticMaterialsChemProp.v5.i1-6

[6] Sellers, J. J., Meerman, M., Paul, M., and Sweeting, M., "A Low-Cost Propulsion Option for Small Satellites," *Journal of the British Interplanetary Society*, Vol. 48, No. 3, 1995, pp. 129–138.

[7] Mechentel, F., and Cantwell, B., "Small-Scale Gaseous Oxygen Hybrid Rocket Testing Facility Upgrades for Regression Rate and Combustion Efficiency Studies," AIAA Paper 2018-4439, July 2018. https://doi.org/10.2514/6.2018-4439

[8] Munjal, N., and Parvatiyar, M., "Ignition of Hybrid Rocket Fuels with Fuming Nitric Acid as Oxidant," *Journal of Spacecraft and Rockets*, Vol. 11, No. 6, 1974, pp. 428–430. https://doi.org/10.2514/3.62093

[9] Tsujikado, N., and Ishihara, A., "90% Hydrogen Peroxide/Polyethylene Hybrid Rocket," *International Journal of Energetic Materials and Chemical Propulsion*, Vol. 7, No. 4, 2008, pp. 263–280. https://doi.org/10.1615/IntJEnergeticMaterialsChemProp.v7.i4

[10] Jain, S., "Self-Igniting Fuel-Oxidizer Systems and Hybrid Rockets," *Journal of Scientific & Industrial Research*, Vol. 62, April 2003, pp. 293–310.

[11] Pfeil, M., Kulkarni, A., Ramachandran, P., Son, S., and Heister, S., "Solid Amine-Boranes as High-Peformance and Hypergolic Hybrid Rocket Fuels," *Journal of Propulsion and Power*, Vol. 32, No. 1, Oct. 2016, pp. 23–31. https://doi.org/10.2514/1.B35591

[12] Pfeil, M., Dennis, J., Son, S., Heister, S., Pourpoint, T., and Ramachandran, P., "Characterization of Ethylenediamine Bisboraneas a Hypergolic Hybrid Rocket Fuel Additive," *Journal of Propulsion and Power*, Vol. 31, No. 1, 2015, pp. 365–372. https://doi.org/10.2514/1.B35386

[13] Jung, E., and Kwon, S., "Autoignitable and Restartable Hybrid Rockets Using Catalytic Decomposition of an Oxidizer," *Journal of Propulsion and Power*, Vol. 30, No. 2, March 2014, pp. 514–518. https://doi.org/10.2514/1.B34739

[14] Wernimont, E., and Heister, S., "Combustion Experiments in Hydrogen Peroxide/Polyethylene Hybrid Rocket with Catalytic Ignition," *Journal of Propulsion and Power*, Vol. 16, No. 2, May 2000, pp. 318–326. https://doi.org/10.2514/2.5571

[15] Huh, J., Jyoti, B., Yun, Y., Shoaib, M., and Kwon, S., "Preliminary Assessment of Hydrogen Peroxide Gel as an Oxidizer in a Catalyst Ignited Hybrid Thruster," *International Journal of Aerospace Engineering*, Vol. 2018, Dec. 2018, Article 5630587. https://doi.org/10.1155/2018/5630587

[16] Dyrda, D., Korneyeva, V., and Cantwell, B., "Diode Laser Ignition Mechanism for Hybrid Propulsion Systems," AIAA Paper 2019-3833, Aug. 2019. https://doi.org/10.2514/6.2019-3833

[17] Jenkins, R., Cruit, W., and Smith, A., "Cold-Flow Study of Hybrid Rocket Motor Flow Dynamics," AIAA Paper 1996-2843, July 1996. https://doi.org/10.2514/6.1996-2843

[18] Karabeyoglu, A., and Zilliac, G., "Hybrid Rocket Fuel Regression Rate Data and Modeling," AIAA Paper 2006-4504, July 2006. https://doi.org/10.2514/6.2006-4504

[19] Jens, E., Karp, A., Williams, K., Nakazono, B., Rabinovitch, J., Dyrda, D., and Mechentel, F., "Low Pressure Ignition Testing of a Hybrid SmallSat Motor," AIAA Paper 2019-4009, Aug. 2019. https://doi.org/10.2514/6.2019-4009

[20] Whitmore, S., Inkley, N., Merkley, D., and Judson, M., "Development of a Power-Efficient, Restart-Capable Arc Ignitor for Hybrid Rockets," *Journal of Propulsion and Power*, Vol. 31, No. 6, 2015, pp. 1739–1749. https://doi.org/10.2514/1.B35595

J. M. Seitzman
Associate Editor